Geophysical Research Letters

RESEARCH LETTER
10.1029/2018GL078218

Key Points:
- The first simultaneous radar and rocket observations of weak, low, and rare polar mesospheric summer clouds were obtained
- The majority of the dust particles appear to be neutral but with a net positive dust charge density
- Size sorting of dust must take place

Correspondence to:
O. Havnes,
ove.havnes@uit.no

Citation:
Havnes, O., Latteck, R., Hartquist, T. W., & Antonsen, T. (2018). First simultaneous rocket and radar detections of rare low summer mesospheric clouds. *Geophysical Research Letters, 45*, 5727–5734. https://doi.org/10.1029/2018GL078218

Received 5 APR 2018
Accepted 24 MAY 2018
Accepted article online 30 MAY 2018
Published online 10 JUN 2018

First Simultaneous Rocket and Radar Detections of Rare Low Summer Mesospheric Clouds

O. Havnes[1], R. Latteck[2], T. W. Hartquist[3], and T. Antonsen[1]

[1]Institute of Physics and Technology, Arctic University of Norway, Tromsø, Norway, [2]Institute of Atmospheric Physics, Kühlungsborn, Germany, [3]School of Physics and Astronomy, University of Leeds, Leeds, UK

Abstract On 30 June 2016 a layer of dust, possibly meteoric smoke particles (MSPs), was observed with a rocket borne probe at 69.29°N, 16.02°E and altitudes of ~74 km where patchy thin cloud layers, detected with the Middle Atmosphere Alomar Radar System, were present. The rocket traversed a layer with a net positive dust charge density of ~10^7 unit charges per cubic meters and a number density of neutral dust particles with sizes ≥4 nm of ~10^8 m^{-3}. The positive charge density may require that elements that lower the photoelectric work function coat MSPs. The presence of this relatively large dust is consistent with smaller MSPs being swept out of the low mesospheric cloud region during the summer, while larger MSPs remain where their fall velocities equals the circulation updraught velocities. Large MSPs initially embedded in icy particles that subsequently sublimate may also fall until their fall velocities match the updraught velocities.

Plain Language Summary A rocket and radar campaign was conducted in the summer of 2016 to investigate the clouds in the Earth's polar middle atmosphere and the role of meteoric smoke particles. They are produced by meteorites entering the atmosphere at high velocities, where they are heated by friction and ablate. We lack knowledge of the cloud transition phases from winter to summer conditions in late May and back in late August. Recent radar observations show that contrary to the belief a few years back, weak and low clouds are not totally absent in the summer season. One of the rockets flew through a very weak and low cloud, which also was observed by radar. The probability for this to happen is very low. Analysis shows that the cloud consists of 4- to 5-nm-sized meteoric smoke particles of number density a few times 10^8 particles m^{-3} with a low positive dust charge density of ~10^7 m^{-3}. Our findings are consistent with size sorting being active and important in the low cloud region especially during the transition phases. The positive charge density apparently requires that the photoelectric properties of the smoke particles are affected by coating with or absorption of gases.

1. Introduction

The various clouds in the Earth's mesosphere have traditionally been classified as either summer clouds or winter clouds. With clouds we mean (mesospheric) dust clouds. The only visually observable clouds are the noctilucent clouds at altitudes of ~80 to ~90 km. They consist of icy particles with sizes up to ~100 nm (Von Cossart et al., 1999). Other clouds that are detected with radars are called polar mesospheric summer echoes (PMSEs; Ecklund & Balsley, 1981) and polar mesospheric winter echoes (PMWEs; Czechowsky et al., 1979). Mesospheric radar echoes, probably formed by turbulence linked to Kelvin-Helmholtz instabilities, are observed at sites close to the equator (Lehmacher et al., 2007).

The NLC/PMSE season starts when the mesopause temperature changes from a winter temperature around 200–220 K to a summer temperature as low as 110–130 K (Lübken, 1999; Von Zahn & Meyer, 1989). The change arises from seasonal variations in the global atmospheric circulation pattern, with the onset of a polar updraught and associated adiabatic cooling. Water vapor then condenses, most likely on meteoric smoke particles (MSPs) (Hervig et al., 2012; Rapp & Thomas, 2006; Rosinski & Snow, 1961).

The PMWEs are much weaker than the PMSEs and occur less frequently. Observed with standard MST radars they disappear in late May and reappear at the beginning of September (Zeller et al., 2006). Since 2011 a new MST radar MAARSY has been in operation at Andøya Rocket Range, Norway. MAARSY has 20 times the power and ~half the beam width of the ALOMAR Wind radar (ALWIN) it replaced (Latteck et al., 2012). The MAARSY observations give significantly different statistics for the PMWEs. One difference is that although the PMWEs become rarer toward the end of the standard PMWE season in May, weak radar scattering layers are occasionally observed with MAARSY during the summer months, at altitudes well below the main NLC/PMSE altitudes (Latteck & Strelnikova, 2015). The temperatures at these lower altitudes are high enough to remove icy particles.

In the following we will call these weak summer echoes rare low summer echoes (RLSEs). This to emphasize that they are different from the much stronger NLC/PMSE, which in summer are nearly always present above the RLSE heights, and further that they differ from the PMWE by being weaker with a much lower occurrence frequency. If dust particles are present in and active in creating the PMWEs, and also the RLSEs, they must be nonvolatile and differ from the icy particles of the NLC/PMSE clouds. MSPs are obvious candidates.

Support for the conjecture that MSPs are involved in creating the PMWEs comes from observations of the radar overshoot effect (Havnes, 2004). The overshoot is produced by the use of artificial periodic RF heating of electrons (Rietveld et al., 1993). The overshoot effect, first observed for NLC/PMSE clouds (Havnes et al., 2003), has also been observed for PMWEs with the European Incoherent Scatter scientific association 224-MHz radar (Belova et al., 2008; Kavanagh et al., 2006; Kero et al., 2008) and the Mobile Radar and Rocket Observatory (MORRO) 56-MHz radar (Havnes et al., 2011; La Hoz & Havnes, 2008). The weak RLSEs that are detected occasionally with MAARSY have not been detected with either of these other radars, which are collocated with the European Incoherent Scatter Heating Facility.

There is no heating facility at the MAARSY site. Consequently, the radar overshoot effect cannot be studied with MAARSY, which has left open several questions about the RLSE clouds. Are they, like the NLC/PMSE and PMWE clouds, controlled by dust particles? If so, are the RLSE particles those remnants of PMWE dust that have not been swept out of the lower mesosphere by the summer updraught? Are they related to the particles in the higher NLC/PMSE clouds? Is it possible that the NLC/PMSE icy particles, when sublimating as they sink to warmer altitudes, release a sufficient number of large MSPs that can overcome the updraught, fall below the NLC/PMSE clouds, and become important charge carriers in RLSE clouds? These are among the many questions requiring answers for an understanding of the transport and role of MSPs, from their creation in the upper mesosphere until they are deposited on the Earth's surface (Plane, 2012), to emerge.

The first step, which can be achieved with rocket borne probes, is to establish whether dust exists in RLSE clouds. However, the rarity of RLSEs presents a challenge.

Below we present, and provide an analysis of data for a RLSE layer that is the first to be detected simultaneously with radar and a rocket borne probe. In section 2 we provide the data. In section 3 we report on the analysis of the data obtained with the probe to find the RLSE dust density and dust charge density, and section 4 contains a discussion and conclusions.

2. The MAXIDUSTY Campaign

During the MXD-1 payload launch on 30 June 2016 at $09^h\ 43^m\ 18^s$ UT, a weak RLSE layer was detected with a DUSTY probe and the MAARSY radar. Though it is always small, the probability for RLSEs to be detectable with MAARSY is largest at the beginning of the NLC/PMSE season and falls significantly by the end of June (Latteck & Strelnikova, 2015). Usually, hardly any detectable RLSEs would be expected when MXD-1 was launched.

Disturbed magnetospheric conditions increase the electron density and the fraction of negatively charged dust and are normally required for PMWEs to be detectable with standard MST radars (Zeller et al., 2006). However, the sensitivity of MAARSY is 17 dB greater than that of ALWIN, a typical MST radar operated at Andøya until 2008. This enabled the detection of RLSEs during quiet magnetospheric, but sunlit, conditions obtained during the MXD-1 flight.

We focus on the DUSTY and MAARSY measurements in the height region below the NLC/PMSE altitudes. The MXD-1 DUSTY probe (Havnes et al., 1996, 2015) is bucket shaped with three grids and a bottom impact plate (BP). Only the currents I_{G2} to the lowest grid G2 and I_{BP} to BP are used since they, being screened from the ambient plasma, are the grids with significant dust impact currents. Figure 1a shows I_{G2} and Figure 1d I_{BP} for the upward trajectory. The main NLC/PMSE are easily identified at altitudes from approximately 81 to 86 km, but there are no clear indications of any RLSEs below these main clouds. However, zooming in on I_{BP} and I_{G2} in the region from 66 to 78 km, as shown in Figures 1b and 1c, we see small changes in the currents up to ~5 pA. This is less than ~1% of the current changes when the NLC/PMSE clouds were traversed.

Near the time t_{74}, MAARSY detected thin patchy RLSEs in the altitude region around 74 km. Figure 2 shows results for four MAARSY beams at 0°, 4°, 8°, and 12° from the vertical toward the azimuth of the rocket trajectory. All beams contained one relatively strong RLSE layer (which was not traversed by the rocket), which

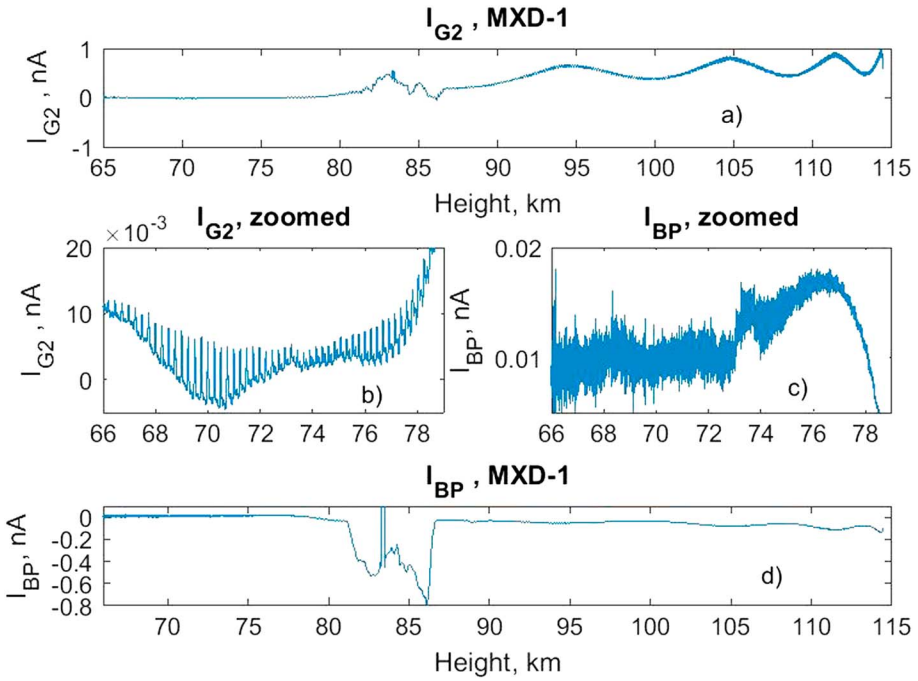

Figure 1. (a and d) The observed current I_{G2} and I_{BP} for altitudes up to apogee. (b and c) Zoom in on the altitude range of the rare low summer echo layer. The disturbance in Figures 1a and 1d at ~83 km is due to the firing of a squib for another instrument.

moved to the north-west and descended. In the MAARSY 12° beam at t_{74}, we see another weaker and more complex RLSE, which was traversed by and detected by rocket instrumentation.

The raw data shown in Figures 1 and 3 contain electronic noise and payload rotation effects. In addition to this we see in the upper heights of Figure 1a, the effect rocket precession with a period ~19.5 s.

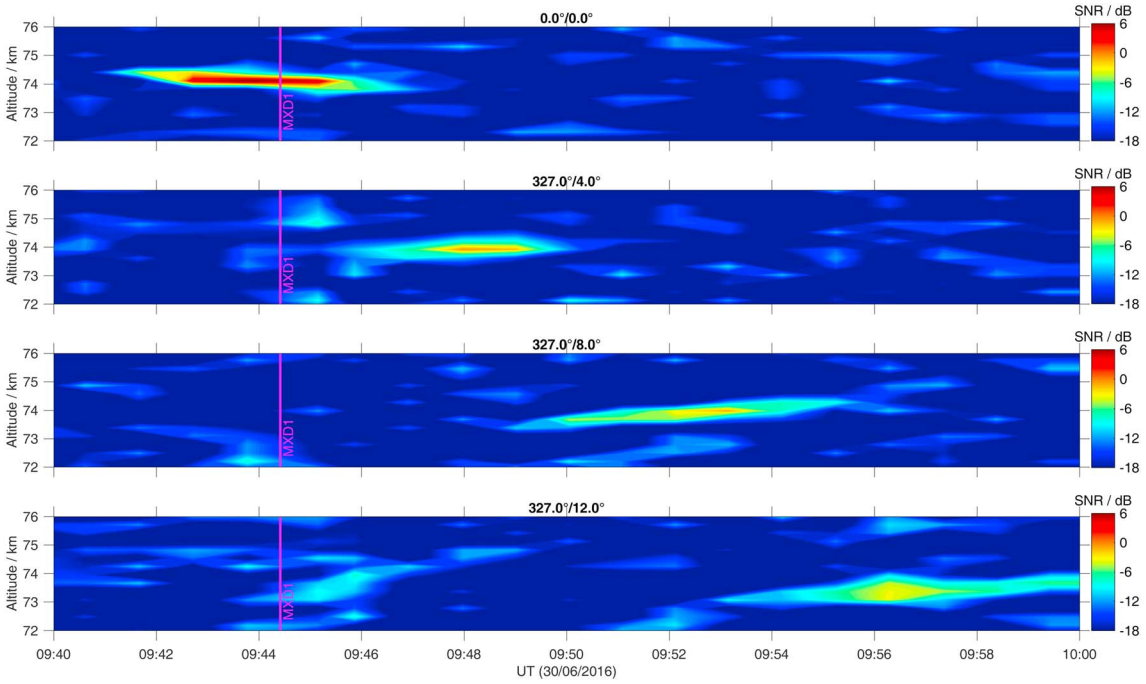

Figure 2. This figure shows results for MAARSY beams in the vertical direction and in directions toward the azimuth of the rocket trajectory at angles of 4°, 8°, and 12° from the vertical. The 12° beam was closest to the rocket trajectory, which passed 74-km height at the time $t_{74} = 09^{h}\ 44^{m}\ 25^{s}$, as indicated by the vertical line. SNR = signal-to-noise ratio.

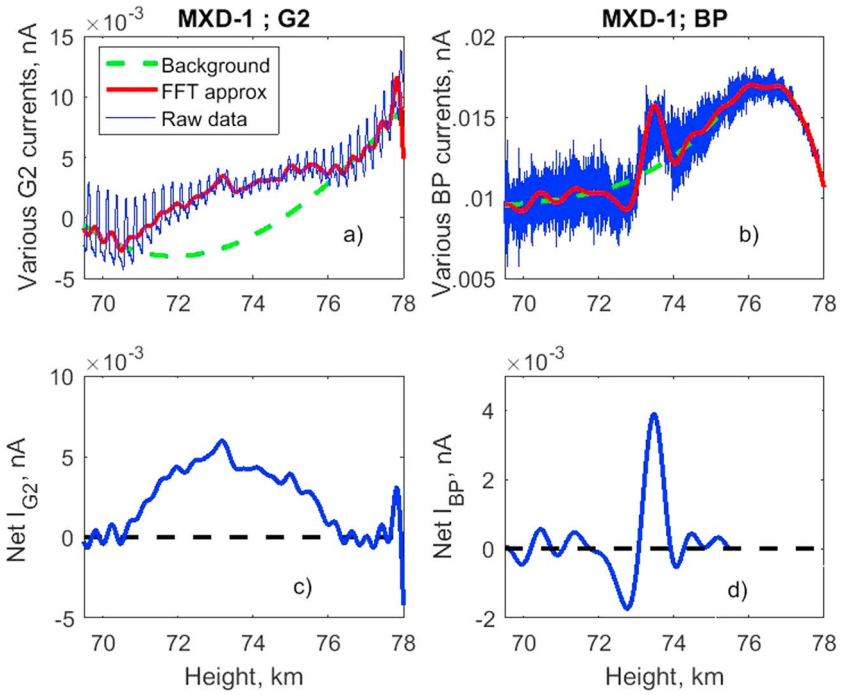

Figure 3. (a and b) The raw current to G2 and bottom impact plate (BP), respectively, the fast Fourier transform (FFT) approximations to the currents and the assumed background currents. (c and d) The net currents to G2 and BP.

Extrapolating this backward in time we find that there should be a minimum effect of the precession at height ~72 km. Without dust we would expect a mean current as shown by the background (green line) in Figure 3a. The actual observations in this height region show that there must have been dust impacts on G2 creating positive currents to it by direct deposition or by rubbing off electrons. To find the net currents to G2 and BP in the RLSE, we used fast Fourier transform (FFT) on the raw currents and an inverse FFT with a cutoff in frequency to remove payload spin effects at ~ 4.5 rps and higher frequency noise. The inverse FFT curves, representing the observations, are shown in Figures 3a and 3b as are the adopted background currents, which we found by interpolating with a third-degree polynomial fitted to altitude regions below (69–70.6 km) and above (76.2–77.5 km) the observed RLSE layer. In Figures 3c and 3d we show the final net currents I_{G2} and I_{BP} where the background has been subtracted.

3. Analysis of the RLSE Observations

The currents I_{BP} and I_{G2} measured with the DUSTY probe are due to impacts of charged and neutral dust particles. We suppose that in RLSEs, as in PMWEs, the particles are probably MSPs with charge number Z distributed between -1, 0, and +1. Photodetachment (Havnes & Kassa, 2009; Rapp, 2009; Weingartner & Draine, 2001) can at sunlit conditions cause the majority of dust particles to be neutral. Though photoionization may produce a significant number of positively charged dust (Asmus et al., 2015; Havnes et al., 1990; Rapp, 2009; Robertson et al., 2009), the number density of neutral dust particles can be much higher than that of the charged dust particles. In such cases the neutral dust particles can play a major role in determining I_{BP} and I_{G2} by rubbing off negative charge when impacting the grid wires of G2 at glancing angles (Havnes & Næsheim, 2007; Tomsic, 2001). The extraction of negative charges from G2 produces a positive current to G2 and a negative current to BP when they impact it.

A distribution of MSPs sizes can extend to sizes below 0.5 nm (Hunten et al., 1980; Rapp & Thomas, 2006). If a full MSP size distribution had been present in the RLSE cloud, DUSTY would have detected only a fraction of the ambient cloud particles because MSPs below a certain size would be swept away from the DUSTY probe by the airstream around the payload. Hedin et al. (2007) calculated the fraction of impacting dust, which were swept away from DUSTY-like probes at various atmospheric conditions. From their results one can conclude that at ~74 km, the fraction γ of particles with radii of 3, 4, and 5 nm that entered DUSTY was 0, 0.4, and 0.7,

respectively. At 74 km the real RLSE particle size distribution will probably differ substantially from the full MSP size distribution because the summer updraught will, within a few weeks after its onset, sweep away the smallest MSPs, while the larger MSPs linger at altitudes at which their fall velocities are comparable to the local updraught velocities (Havnes & Kassa, 2009). MAARSY observations (Latteck & Strelnikova, 2015, Figure 5) showing that RLSEs are found at altitudes from ~60 to ~80 km in the early phases of the NLC/PMSE season but that the lower altitude limit gradually increases with time provide evidence that this is the case. This is consistent with Rapp et al. (2010) not detecting MSPs in the lower RLSE region during the last part of the summer. We attribute this behavior to the lower regions, where fall velocities are smallest, being swept nearly clean of dust first.

Thus, for our analysis we assume that the MSPs can have three different charge states $Z = +1$, 0, and -1 (Asmus et al., 2015). We also assume that at the launch of MXD-1 all of the small particles had been swept out of the RLSE altitude region, while particles with sizes of several nanometers remained present in the upper parts of the RLSE region. Some large MSPs may also have fallen into the upper RLSE regions when sublimating NLC/PMSE particles released their embedded MSPs. In the following we will take the RLSE particle size lower limit to be large enough that the DUSTY probe registered the impact of a major fraction of the charged RLSE particles. Observations for which the dust capture efficiency is lower than 100% would mimic observations with a smaller cross section than that of the real DUSTY.

The flux of positively charged dust in front of G2 is $\Gamma(+)$, that of neutral dust is $\Gamma(0)$, and that of negatively charged dust is $\Gamma(-)$. The current I_{G2} is given by

$$I_{G2} = e\,[\Gamma(+) - \Gamma(-)]\sigma_2 + e\,[\Gamma(+) + \Gamma(0) + \Gamma(-)]\eta\sigma_{2,s} \tag{1}$$

The DUSTY probe is closed to ambient electrons and ions, which do not contribute to I_{G2} or I_{BP}. The first term on the right-hand side of equation (1) is due to positively and negatively charged dust colliding with G2. The second term describes the secondary charging effect due to high impact angle collisions of particles near the edges of the G2 grid wires rubbing off electrons and creating a positive current to G2. The G2 wire thickness and grid density is such that the G2 grid, if projected on to the bottom plate of DUSTY, covers a fraction $\sigma_2 = 0.235$ of it. Glancing impacts that produce secondary charges, occur according to our model (Havnes & Næsheim, 2007) on ~28% of the G2 cross section and $\sigma_{2,s} = 0.28\sigma_2$ is therefore the fraction of the DUSTY cross section that produces secondary charges. The secondary charge production efficiency η, which is proportional to the cross section of the impacting dust particle (see equation (6)), is the average number of unit charges that are rubbed off by dust particles impacting near the G2 wire edges.

The current I_{BP} is given by

$$I_{BP} = e\,[\Gamma(+) - \Gamma(-)](1 - \sigma_2) - e\,[\Gamma(+) + \Gamma(0) + \Gamma(-)]\eta\sigma_{2,s} \tag{2}$$

The first term on the right-hand side is due to the direct dust charge deposition on BP. The second term is caused by electrons that were rubbed off G2 being deposited as a negative current to BP.

The sum of equations (1) and (2) gives the net flux of charged dust in front of G2 as

$$\Gamma\,(\mathrm{Ch}) = \Gamma(+) - \Gamma(-) = (I_{G2} + I_{BP})/e \tag{3}$$

Considering the currents shown in Figures 3c and 3d, we see that Γ (Ch) must be positive. This rules out the ambient electron number density being large compared to the MSP number density since in such circumstances the majority of the MSPs would have $Z = -1$. We ignore this possibility and take the majority of the MSPs to be neutral and moderate fractions of MSPs to have $Z = -1$ and +1. Neglecting $\Gamma(+)$ and $\Gamma(-)$ in comparison with $\Gamma(0)$ in the last term of each of equations (1) and (2) and inserting equation (3) into equation (2) we find that

$$\Gamma(0) = [(1 - \sigma_2)\, I_{G2} - \sigma_2\, I_{BP}]/e\eta\sigma_{2,s} \tag{4}$$

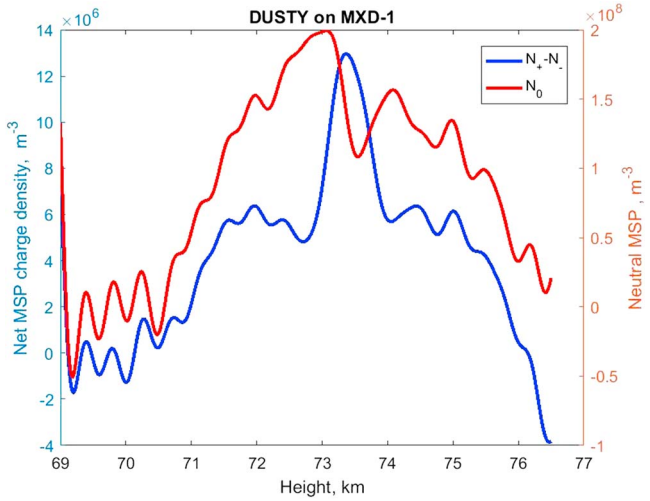

Figure 4. The dust charge density and the total number density $N(0)$ of neutral particles are shown. $N(0)$ is inversely proportional to the secondary charge production factor η. For this figure $\eta = 0.5$. MSP = meteoric smoke particle.

The secondary charge production efficiency is given by

$$\eta = \eta_{\mathrm{ref}} \, (r_{\mathrm{D}}/50)^2 \tag{5}$$

Here r_{D} is the radius of the impacting dust in nanometers. Modeling of rocket observations (Havnes & Næsheim, 2007; Kassa et al., 2012) implies that the reference value η_{ref} is in the range of ~50 to ~100 secondary unit charges produced per impact by a 50-nm-sized NLC/PMSE particle. This is several magnitudes larger than for impacts of pure ice particles (Andersson & Pettersson, 1998; Dubov & Vostrikov, 1991; Tomsic, 2001). This difference can be due to the large number of MSPs embedded in NLC/PMSE particles (Havnes & Næsheim, 2007; Hervig et al., 2012) because when a NLC/PMSE particle collides near the edge of, for example, a grid wire, it fragments and releases embedded MSPs. Pure ice particles smaller than ~7 nm attach to the impact surface and melt (Tomsic, 2001), but nonvolatile MSPs released in the collision do not. Using equation (5) we find that η may be in the range 0.3 to 1 unit charge per impact if we vary η_{ref} from 50 to 100 and the dust radius from 4 to 5 nm.

The ambient number density of the neutral dust $N(0)$ and net ambient dust charge number density, N (Ch) = $N(+) - N(-)$, are

$$N\,(X) = \Gamma\,(X)/\pi R^2 V_R\,(1-\sigma_1)^2 \tag{6}$$

where $X = 0$ or $X =$ Ch and $R = 0.04$ m is the DUSTY probe radius, V_R is the rocket speed (~910 m/s at altitude 74 km) and $\sigma_1 = 0.045$ is the fraction of the DUSTY cross section covered by the two screening grids G1 and G0 at the top of DUSTY. Equation (6) is based on the assumption that none of the RLSE dust particles are deflected away from the probe. Using Γ (Ch) and $\Gamma(0)$ from equations (3) and (4) with $\eta = 0.5$, we find the number densities $N(0)$ and N (Ch) throughout the cloud shown in Figure 4.

We see from a comparison between the radar observations in the 12° beam in Figure 2 and the DUST charge density in Figure 4 that the charged dust layer extends from ~71.5 to 75 km, which is roughly the height range of the radar echo when the payload is at 74-km height. The local maximum in dust charge density at slightly above 73 km also fits well with a local radar echo maximum.

Equations (3) and (4) show that N (Ch) is independent of η and that $N(0)$ is inversely proportional to η. If the effective cross section of DUSTY is smaller than the geometric cross section πR^2 by a factor γ then both N (Ch) and $N(0)$ increase by a factor $1/\gamma$.

4. Discussion and Conclusions

This paper reports the first simultaneous radar and rocket summer observations of the weak and low mesospheric dust clouds (Latteck & Strelnikova, 2015). The observed layer was found to have a net positive dust charge density ~10^7 unit charges per cubic meters and a neutral dust density ~10 times above this. We find that the dust sizes have to be of the order of 4 to 5 nm both to be detectable by the DUSTY probe and to balance the expected updraught. A rough comparison between dust fall velocity (Havnes & Kassa, 2009) and zonal mean upward vertical velocity (Crane et al., 1980) indicates that 4- to 5-nm particles are lifted by the updraught at altitudes below ~70 km but that their fall velocity may balance the updraught velocity at the altitude of the observed RLSE layer. If so, such particles accumulate there. Large MSPs released by sublimating NLC/PMSE icy particles may provide a source of particles in RLSE layers above about 70 km but should not fall much lower.

As mentioned above, the results of Hedin et al. (2007) indicate that at ~74 km all particles with sizes less than ~3 nm would have been deflected away from DUSTY by the airstream around the payload. However, for the particles that updraughts should leave to remain at ~74 km, γ is in the range of 0.4 to 0.7 indicating that the number densities in Figure 4 might be a factor of about 2 too small.

Since many particles in the RLSE layer are charged positively, photodetachment and photoionization must be important. This is consistent with the sunlit conditions during the MXD-1 flight and the finding of Havnes

et al. (2011) that photodetachment was the dominant mechanism returning the dust charges back to equilibrium in PMWE overshoot experiments.

For the photoionization to be effective, the dust work function has to be low. Havnes et al. (1990) suggested that a thin coating of other elements, or trace contaminations on NLC/PMSE dust particles, could lower the work function, as what happens on other substances. For example, Na and NH_3, when codeposited on thin films, result in a work function of only 0.9 eV (Qiu et al., 1989). Small dust particles can also have a much lower work function than the bulk material (Burtscher et al., 1984; Schmidt-Ott et al., 1980). The relevant observational breakthrough is due to Robertson et al. (2014) who, using a new dust mass spectrometer MASS (Knappmiller et al., 2008) launched in October 2011, found coexisting small positive and negative MSPs at altitudes from 60 to 70 km. The possibility that coatings reduce the work function of mesospheric NLC/PMSE particles had previously been discarded with respect to Na contamination because there is not enough contaminating material (Vondrak et al., 2006). However, our RLSE has a total particle surface area per atmospheric volume that is more than 2 orders of magnitude smaller than that in a moderately strong NLC/PMSE cloud, which may lead to a much more complete surface coating and a stronger contamination in the RLSE clouds.

In summary, we find that the following issues are raised by our observations:

1. Size sorting should occur when the updraught starts at the beginning of the summer NLC/PMSE season. How effective is this for MSPs and at what altitudes, as functions of time from the onset of the updraught, are the various particles deposited?
2. The charged particles in the RLSE that we observed are mainly positively charged, which we attribute to a comparatively low electron density and efficient photodetachment and photoionization. In order to gain further insight into RLSE formation, one should aim to launch probes early in the NLC/PMSE season through RLSEs, which are much more common then. We predict that normally a net positive dust charge density will be found in RLSEs when quiet magnetospheric conditions obtain since then the electron density will be low.
3. During high magnetospheric activity the electron density should normally be larger and in such a case we would expect the net dust charge density in a RLSE to be negative.
4. There should be intermediate conditions for which the net dust charge density is small. In such cases we would expect the radar backscatter on RLSEs to be particularly weak. In a plot of RLSE radar strength against magnetospheric activity a local minimum in RLSE strength and occurrence rate may be found between extremely quiet activity and strong activity.

Acknowledgments
The rocket campaign and the construction of the rocket instrumentation was supported by grants from the Norwegian Space Centre (VIT.04.14.7; VIT.02.14.1; VIT.03.15.7; VIT.03.16.7), the Research Council of Norway (240065), and by the Arctic University of Norway. Rocket and radar data for replication of results are available through the UiT Open Research Repository through the DOI https://doi.org/10.18710/PRJW7B.

References

Andersson, P. U., & Pettersson, J. B. (1998). Water cluster collisions with graphite surfaces: Angular-resolved emission of large cluster ions. *The Journal of Physical Chemistry B*, *102*(38), 7428–7433. https://doi.org/10.1021/jp981889x

Asmus, H., Robertson, S., Dickson, S., Friedrich, M., & Megner, L. (2015). Charge balance for the mesosphere with meteoric dust particles. *Journal of Atmospheric and Solar-Terrestrial Physics*, *127*, 137–149. https://doi.org/10.1016/j.jastp.2014.07.010

Belova, E., Smirnova, M., Rietveld, M. T., Isham, B., Kirkwood, S., & Sergienko, T. (2008). First observation of the overshoot effect for polar mesosphere winter echoes during radiowave electron temperature modulation. *Geophysical Research Letters*, *35*, L03110. https://doi.org/10.1029/2007GL032457

Burtscher, H., Schmidt-Ott, A., & Siegmann, H. C. (1984). Photoelectron yield of small silver and gold particles suspended in gas up to a photon energy of 10 eV. *Zeitschrift fur Physik B: Condensed Matter*, *56*(3), 197–199. https://doi.org/10.1007/BF01304172

Crane, A. J., Haigh, J. D., Pyle, J. A., & Rogers, C. F. (1980). Mean meridional circulations of the stratosphere and mesosphere. *Pure and Applied Geophysics*, *118*(1), 307–328. https://doi.org/10.1007/BF01586456

Czechowsky, P., Rüster, R., & Schmidt, G. (1979). Variations of mesospheric structures in different seasons. *Geophysical Research Letters*, *6*(6), 459–462. https://doi.org/10.1029/GL006i006p00459

Dubov, D. Y., & Vostrikov, A. A. (1991). Collision induced electrification of large water clusters. *Journal of Aerosol Science*, *22*, S245–S248. https://doi.org/10.1016/S0021-8502(05)80081-3

Ecklund, W. L., & Balsley, B. B. (1981). Long-term observations of the Arctic mesosphere with the MST radar at poker flat, Alaska. *Journal of Geophysical Research*, *86*(A9), 7775–7780. https://doi.org/10.1029/JA086iA09p07775

Havnes, O. (2004). Polar mesospheric summer echoes (PMSE) overshoot effect due to cycling of artificial electron heating. *Journal of Geophysical Research*, *109*, A02309. https://doi.org/10.1029/2003JA010159

Havnes, O., Antonsen, T., Hartquist, T. W., Fredriksen, Å., & Plane, J. M. C. (2015). The Tromsø programme of in situ and sample return studies of mesospheric nanoparticles. *Journal of Atmospheric and Solar-Terrestrial Physics*, *127*, 129–136. https://doi.org/10.1016/j.jastp.2014.09.010

Havnes, O., de Angelis, U., Bingham, R., Goertz, C. K., Morfill, G. E., & Tsytovich, V. (1990). On the role of dust in the summer mesopause. *Journal of Atmospheric and Terrestrial Physics*, *52*, 637.

Havnes, O., & Kassa, M. (2009). On the sizes and observable effects of dust particles in polar mesospheric winter echoes. *Journal of Geophysical Research*, *114*, D09209. https://doi.org/10.1029/2008JD011276

Havnes, O., La Hoz, C., Næsheim, L. I., & Rietveld, M. T. (2003). First observations of the PMSE overshoot effect and its use for investigating the conditions in the summer mesosphere. *Geophysical Research Letters*, *30*(23), 2229. https://doi.org/10.1029/2003GL018429

Havnes, O., La Hoz, C., Rietveld, M. T., Kassa, M., Baroni, G., & Biebricher, A. (2011). Dust charging and density conditions deduced from observations of PMWE modulated by artificial electron heating. *Journal of Geophysical Research*, *116*, D24203. https://doi.org/10.1029/2011JD016411

Havnes, O., & Næsheim, L. I. (2007). On the secondary charging effects and structure of mesospheric dust particles impacting on rocket probes. *Annales Geophysicae*, *25*, 623–637. https://doi.org/10.5194/angeo-25-623-2007

Havnes, O., Trøim, J., Blix, T., Mortensen, W., Næsheim, L. I., Thrane, E., & Tønnesen, T. (1996). First detection of charged dust particles in the Earth's mesosphere. *Journal of Geophysical Research*, *101*(A5), 10,839–10,847. https://doi.org/10.1029/96JA00003

Hedin, J., Gumbel, J., & Rapp, M. (2007). On the efficiency of rocket-borne particle detection in the mesosphere. *Atmospheric Chemistry and Physics*, *7*(14), 3701–3711. https://doi.org/10.5194/acp-7-3701-2007

Hervig, M. E., Deaver, L. E., Bardeen, C. G., Russell, J. M. III, Bailey, S. M., & Gordley, L. L. (2012). The content and composition of meteoric smoke in mesospheric ice particles from SOFIE observations. *Journal of Atmospheric and Solar-Terrestrial Physics*, *84-85*, 1–6. https://doi.org/10.1016/j.jastp.2012.04.005

Hunten, D. M., Turco, R. P., & Toon, O. B. (1980). Smoke and dust particles of meteoric origin in the mesosphere and stratosphere. *Journal of the Atmospheric Sciences*, *37*(6), 1342–1357. https://doi.org/10.1175/1520-0469(1980)037%3C1342:SADPOM%3E2.0.CO;2

Kassa, M., Rapp, M., Hartquist, T. W., & Havnes, O. (2012, March). Secondary charging effects due to icy dust particle impacts on rocket payloads. *Annales Geophysicae*, *30*(3), 433–439. https://doi.org/10.5194/angeo-30-433-2012

Kavanagh, A. J., Honary, F., Rietveld, M. T., & Senior, A. (2006). First observations of the artificial modulation of polar mesospheric winter echoes. *Geophysical Research Letters*, *33*, L19801. https://doi.org/10.1029/2006GL027565

Kero, A., Enell, C. F., Kavanagh, A. J., Vierinen, J., Virtanen, I., & Turunen, E. (2008). Could negative ion production explain the polar mesosphere winter echo (PMWE) modulation in active HF heating experiments? *Geophysical Research Letters*, *35*, L23102. https://doi.org/10.1029/2008GL035798

Knappmiller, S., Robertson, S., Sternovsky, Z., & Friedrich, M. (2008). A rocket-borne mass analyzer for charged aerosol particles in the mesosphere. *Review of Scientific Instruments*, *79*(10), 104502. https://doi.org/10.1063/1.2999580

La Hoz, C., & Havnes, O. (2008). Artificial modification of polar mesospheric winter echoes with an RF heater: Do charged dust particles play an active role? *Journal of Geophysical Research*, *113*, D19205. https://doi.org/10.1029/2008JD010460

Latteck, R., Singer, W., Rapp, M., Vandepeer, B., Renkwitz, T., Zecha, M., & Stober, G. (2012). MAARSY: The new MST radar on Andøya—System description and first results. *Radio Science*, *47*, RS1006. https://doi.org/10.1029/2011RS004775

Latteck, R., & Strelnikova, I. (2015). Extended observations of polar mesosphere winter echoes over Andøya (69°N) using MAARSY. *Journal of Geophysical Research: Atmospheres*, *120*, 8216–8226. https://doi.org/10.1002/2015JD023291

Lehmacher, G. A., Guo, L., Kudeki, E., Reyes, P. M., Akgiray, A., & Chau, J. L. (2007). High-resolution observations of mesospheric layers with the Jicamarca VHF radar. *Advances in Space Research*, *40*(6), 734–743. https://doi.org/10.1016/j.asr.2007.05.059

Lübken, F. J. (1999). Thermal structure of the Arctic summer mesosphere. *Journal of Geophysical Research*, *104*(D22), 27,803–27,810. https://doi.org/10.1029/1999JD900076

Plane, J. M. C. (2012). Cosmic dust in the Earth's atmosphere. *Chemical Society Reviews*, *41*(19), 6507–6518. https://doi.org/10.1039/C2CS35132C

Qiu, S. L., Lin, C. L., Jiang, L. Q., & Strongin, M. (1989). Photoemission studies of the metal-nonmetal transition of sodium on solid ammonia. *Physical Review B*, *39*(3), 1958–1961. https://doi.org/10.1103/PhysRevB.39.1958

Rapp, M. (2009). Charging of mesospheric aerosol particles: The role of photodetachment and photoionization from meteoric smoke and ice particles. *Annales Geophysicae*, *27*(6), 2417–2422. https://doi.org/10.5194/angeo-27-2417-2009

Rapp, M., Strelnikova, I., Strelnikov, B., Hoffmann, P., Friedrich, M., Gumbel, J., et al. (2010). Rocket-borne in situ measurements of meteor smoke: Charging properties and implications for seasonal variation. *Journal of Geophysical Research*, *115*, D00I16. https://doi.org/10.1029/2009JD012725

Rapp, M., & Thomas, G. E. (2006). Modeling the microphysics of mesospheric ice particles: Assessment of current capabilities and basic sensitivities. *Journal of Atmospheric and Solar-Terrestrial Physics*, *68*(7), 715–744. https://doi.org/10.1016/j.jastp.2005.10.015

Rietveld, M. T., Kohl, H., Kopka, H., & Stubbe, P. (1993). Introduction to ionospheric heating at Tromsø—I. Experimental overview. *Journal of Atmospheric and Terrestrial Physics*, *55*(4–5), 577–599. https://doi.org/10.1016/0021-9169(93)90007-L

Robertson, S., Dickson, S., Horányi, M., Sternovsky, Z., Friedrich, M., Janches, D., et al. (2014). Detection of meteoric smoke particles in the mesosphere by a rocket-borne mass spectrometer. *Journal of Atmospheric and Solar-Terrestrial Physics*, *118*, 161–179.

Robertson, S., Horányi, M., Knappmiller, S., Sternovsky, Z., Holzworth, R., Shimogawa, M., et al. (2009). Mass analysis of charged aerosol particles in NLC and PMSE during the ECOMA/MASS campaign. *Annales Geophysicae*, *27*, 1213–1232. https://doi.org/10.5194/angeo-27-1213-2009

Rosinski, J., & Snow, R. H. (1961). Secondary particulate matter from meteor vapors. *Journal of Meteorology*, *18*(6), 736–745. https://doi.org/10.1175/1520-0469(1961)018%3C0736:SPMFMV%3E2.0.CO;2

Schmidt-Ott, A. P. H. C., Schurtenberger, P., & Siegmann, H. C. (1980). Enormous yield of photoelectrons from small particles. *Physical Review Letters*, *45*(15), 1284. https://doi.org/10.1103/PhysRevLett.45.1284

Tomsic, A. (2001). Collisions between water clusters and surfaces, PhD thesis, Gothenburg University.

Von Cossart, G., Fiedler, J., & Von Zahn, U. (1999). Size distributions of NLC particles as determined from 3-color observations of NLC by ground-based lidar. *Geophysical Research Letters*, *26*(11), 1513–1516. https://doi.org/10.1029/1999GL900226

Von Zahn, U., & Meyer, W. (1989). Mesopause temperatures in polar summer. *Journal of Geophysical Research*, *94*(D12), 14,647–14,651. https://doi.org/10.1029/JD094iD12p14647

Vondrak, T., Plane, J. M. C., & Meech, S. R. (2006). Photoemission from sodium on ice: A mechanism for positive and negative charge coexistence in the mesosphere. *The Journal of Physical Chemistry B*, *110*(9), 3860–3863. https://doi.org/10.1021/jp0571630

Weingartner, J. C., & Draine, B. T. (2001). Electron-ion recombination on grains and polycyclic aromatic hydrocarbons. *The Astrophysical Journal*, *563*(2), 842. https://doi.org/10.1086/324035–852

Zeller, O., Zecha, M., Bremer, J., Latteck, R., & Singer, W. (2006). Mean characteristics of mesosphere winter echoes at mid- and high-latitudes. *Journal of Atmospheric and Solar-Terrestrial Physics*, *68*(10), 1087–1104. https://doi.org/10.1016/j.jastp.2006.02.015